Nanotechnology **18** (2007) 285702 (6pp) doi:10.1088/0957-4484/18/28/285702

Collapse analysis of nanofibres

Xiang-Fa Wu and Yuris A Dzenis

Department of Engineering Mechanics, Nebraska Center for Materials and Nanoscience, University of Nebraska-Lincoln, Lincoln, NE 68588-0526, USA

E-mail: xfwu@unlserve.unl.edu

Received 18 January 2007, in final form 22 April 2007
Published 15 June 2007
Online at stacks.iop.org/Nano/18/285702

Abstract

Continuous nanofibres fabricated by the electrospinning technique have found increasing applications (e.g. nanofibre composites, nanofibre devices, bioengineering tissue scaffolding, etc). For a nanofibre network subjected to a small external perturbation, the fibre segments within the network may deflect and stick to each other under the condition that their surface adhesion energy overcomes the elastic strain energy induced by fibre bending. Therefore, this paper aims to study adhesion-induced nanofibre collapse and relevant criteria. A simple fibre collapse model was proposed, which is based on the contact of two deflected elastic filaments under surface adhesion. Four fundamental fibre collapse modes (i.e. fibre-flat substrate, parallel fibres, orthogonal fibres and fibres at arbitrary angle) were considered, and corresponding collapse criteria were determined in explicit forms. Effects of fibre elasticity, surface adhesion and fibre geometries on the collapse criterion were explored in a numerical manner. Results show that for a fibre segment pair at a relatively large angle, the critical distance to induce the fibre collapse is independent of the fibre radius. This distance is a function of the fibre aspect ratio and the material intrinsic length (γ/E, where γ is the surface energy and E is Young's modulus). The fibre collapse model developed in this study can be used as the theoretical basis for design and failure analysis of nanofibre networks and nanofibre devices, among others.

(Some figures in this article are in colour only in the electronic version)

1. Introduction

Due to their porous properties with high surface area to volume ratio and tensile strength, fibrous materials have found extensive applications in thermal and sound insulators, gas and fluid filters, electromagnetic shields, chemical carriers, tissue templates, paper products, fibrous reinforcement in composites, etc. The effective properties of a fibrous material are a result of the properties of individual fibres, fibre arrangement and bonding strength between neighbouring fibre segments in contact. By comparison with their bulk counterparts, fibres typically have higher tensile strength that can be further enhanced with decreasing their diameters under proper spinning conditions. As a result, fibre networks made of ultrathin fibres (e.g. nanofibres) are expected to bear preferable chemophysical and mechanical properties superior to those made of thicker fibres. Recently, ultrathin continuous fibres with diameters ranging from hundreds of nanometres up to a few microns have been fabricated successfully by means of the electrospinning technique [1–3]. As one of the novel nanomanufacturing methods, electrospinning is capable of producing clean and uniform ultrathin fibres from various precursors (e.g. polymers, biomaterials, ceramics, etc). Figure 1 shows typical electrospun polyacrylonitrile (PAN) nanofibres with diameters around 300 nm. Furthermore, ultrathin fibres with diameters lower than 5 nm have also been produced successfully by electrospinning [4]. So far, continuous nanofibres have found rapidly growing applications in nanofibre composites [5–8], ultrafine filtration, chemical carriers [9], biomedical engineering and biological technology [9–11], among others.

In view of mechanics, fibre networks (assemblies) belong to heterogeneous material. Subjected to external loading, the global mechanical response of a fibre network depends upon the specific fibre arrangement, interaction between neighbouring fibres (e.g. contact, adhesion, friction, etc) and the mechanical properties of individual fibres. For effective stiffness of fibre networks, remarkable progress has been

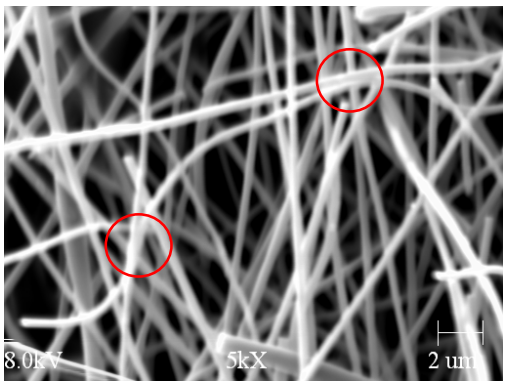

Figure 1. Adhesion between nanofibres within PAN nanofibre network (nanofibre diameter: ∼300 nm, circles indicate the adhesion zones).

made since the pioneering work by van Wyk [12] and Cox [13]. Quite a few models [14–33] have been developed in the last two decades based on various assumptions of fibre deformations and fibre–fibre contacts. These models were largely validated in experiments and/or purely numerical simulations (e.g. FEA). On the other hand, with decreasing fibre diameters, fibre rigidity decays rapidly and the fibre surface effect may play an appreciable role in the mechanical response of fibre networks such as effective stiffness, flexural rigidity, dynamic properties (e.g. wave dispersion [34]), among others.

Consider a fibre network made of thin fibres subjected to small perturbation (e.g. air flow). Neighbouring fibres in the network may deflect and stick to each other due to their low flexural rigidity and appreciable surface adhesion. As a result, fibre collapse and adhesion vary the connectivity and topology of the fibre network, and may further lead to nonlinear behaviour and even global collapse (e.g. large area adhesion) of the fibre network. As a matter of fact, fibre collapse and adhesion definitely degrades the superior properties of fibre networks that are based on their unique fibrous geometries. Furthermore, nanofibre collapse and adhesion may even lead to the catastrophic failure of single nanofibre devices to be developed. Therefore, it is desired to explore the collapse mechanisms and relevant criteria in order to predict and therefore avoid the catastrophic failure of nanofibre networks and nanofibre devices. Nevertheless, to the authors' knowledge, no study has been reported yet in the literature to take into account nanofibre collapse.

Thus, in this work we initiate the study to consider surface adhesion-induced collapse and relevant criteria of thin fibres in a fibre network. A simple fibre collapse model is proposed, which is based on the contact of two deflected elastic cylindrical filaments involving surface energy. For the study of adhesion between elastic bodies, several pioneering models (e.g. DMT, JKR, Maugis–Dugdale, etc) have been proposed and validated in experiments [35–39]. Comparison among these models and their applications in MEMS/NEMS were reviewed in the recent literature [40, 41]. For our purpose, Bradley's approach [35] is to be employed for determining the adhesive force between neighbouring fibre segments sticking at one point. Four fundamental collapse modes (i.e. fibre-flat substrate, parallel fibres, orthogonal fibres and fibres at arbitrary angle) are to be considered. For each case, corresponding collapse criterion is obtained in explicit form. Effects of fibre elasticity, surface energy and fibre geometries on the collapse criterion are explored in detail using a numerical manner. Potential applications of the present model in design and failure analysis of fibre networks and nanofibre devices are further addressed.

2. Problem statement and solutions

In this work, we are going to focus on the fibre collapse in a fibre network induced by surface adhesion between neighbouring fibre segments. The typical nanofibre network formed in electrospinning is shown in figure 1, in which PAN nanofibres stick together at some locations due to surface adhesion. Without loss of generality, two assumptions will be implied in the upcoming derivation to simplify the modelling process. First, each fibre segment is assumed to be fixed between neighbouring contacts, and the contacts have no displacements during the deflection of fibre segments, i.e. each fibre segment is considered simply as a fixed beam. Second, surface adhesion between neighbouring fibre segments is assumed ideal, i.e. fibres are dealt with as ideal elastic cylinders and effects of surface roughness and environmental factors (e.g. moisture) are ignored. Therefore, in the present case of typical electrospun nanofibres with diameters over hundreds of nanometres, classic adhesion theories can be safely used. In this study, four fundamental fibre collapse modes are to be considered (i.e. fibre-flat substrate, parallel fibres, orthogonal fibres and fibres at arbitrary angle), respectively, in which surface adhesion between fibre and flat substrate can be considered as the limiting case of the other three.

2.1. Collapse of nanofibre segment on flat substrate

First consider the adhesion-induced collapse of a fibre segment on flat substrate. The fibre segment is assumed to be fixed at a distance h evenly to the flat substrate, with length L and radius r, as shown in figure 2(a). The fibre material is regarded as linearly isotropic elastic with Young's modulus E. At sufficiently small distance h, subjected to small perturbation (e.g. air flow, dust collision, etc), the fibre segment may collapse and stick to the substrate due to the adhesive force, as illustrated in figure 2(b). At the critical condition of one-point contact, deflection of the mid-span of the fibre segment is h, as shown in figure 2(c). Based on elementary Euler–Bernoulli beam theory, the deflection v and corresponding adhesive force P required in inducing the collapse can be expressed as

$$v = 3h\left[\left(\frac{2x}{L}\right)^2 - \frac{2}{3}\left(\frac{2x}{L}\right)^3\right], \tag{1}$$

$$P = \frac{48\pi Er^4 h}{L^3}. \tag{2}$$

In the above, due to the symmetry of the fibre deflection, x can be understood as the distance from an arbitrary point on the fibre segment to the fixed support or equivalently the distance from that to the contact point, as shown in figure 2(c). Relation (2) is to be used in determining the critical collapse distance h_c once the adhesive force P is estimated. As we

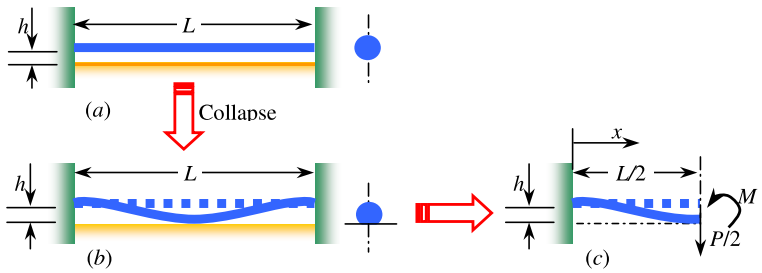

Figure 2. Adhesion between fibre segment and flat substrate.

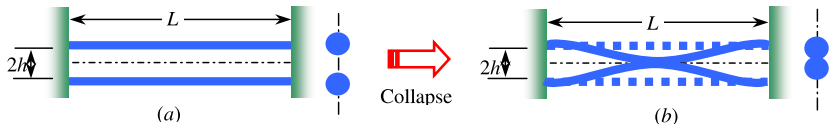

Figure 3. Adhesion between parallel fibre segments.

know, the adhesive forces between two fibre segments are actually distributed. However, they can be replaced by their resultant P due to the rapidly decaying characteristic of the adhesive force with increasing gap between two fibres near the contact point. Furthermore, the adhesive force P can be directly calculated using Bradley's approach [35], which is based on the long-range Lennard-Jones force between two unit areas [42], i.e.

$$\sigma(z) = \frac{8\Delta\gamma}{3\varepsilon}\left[\left(\frac{\varepsilon}{z}\right)^3 - \left(\frac{\varepsilon}{z}\right)^9\right]. \tag{3}$$

Here, ε is a phenomenological distance between two atoms/molecules; z is the distance between two unit areas; and $\Delta\gamma$ is the Dupré adhesion energy [43] that is defined as

$$\Delta\gamma = \gamma_1 + \gamma_2 - \gamma_{12}, \tag{4}$$

where γ_1 and γ_2 are, respectively, the surface energies of the nanofibre and the substrate and γ_{12} is the interface energy between the nanofibre and the flat substrate. According to Bradley's approach [35], the deflected nanofibre segment can be regarded as rigid at the critical condition of one-point contact (see figure 2(c)). Therefore, with the aid of the deflection shape (1), the asymptotic distance between the deflected fibre segment and the flat substrate near the contact point can be expressed as

$$z = 3h\left[\left(\frac{2x}{L}\right)^2 - \frac{2}{3}\left(\frac{2x}{L}\right)^3\right] + \frac{y^2}{2r} + h_0$$
$$\approx 3h\left(\frac{2x}{L}\right)^2 + \frac{y^2}{2r} + h_0, \qquad (\text{for } x/L \ll 1) \tag{5}$$

where h_0 is the minimum gap at the contact point after collapse, which can be selected as $h_0 = \varepsilon$ according to Bradley's approach [35]. x and y are the coordinates of an arbitrary point on the substrate with x axis along the fibre axis and y axis perpendicular to the fibre axis in the horizontal plane. As a result, the adhesive force P can be determined:

$$P = 4\int_A \sigma(z)\,\mathrm{d}A$$
$$= \frac{32\Delta\gamma}{3\varepsilon}\int_0^{+\infty}\int_0^{+\infty}\left[\left(\frac{\varepsilon}{z}\right)^3 - \left(\frac{\varepsilon}{z}\right)^9\right]\mathrm{d}x\,\mathrm{d}y,$$
$$= \frac{\pi}{\sqrt{6}}\Delta\gamma L\sqrt{r/h}, \tag{6}$$

where geometrical symmetry of the contact zone and $h_0 = \varepsilon$ have been implied. Substituting (6) into (2) yields the critical collapse distance h_c:

$$\left(\frac{h_c}{L}\right)^{3/2} = \frac{1}{48\sqrt{6}}\frac{\Delta\gamma}{Er}\left(\frac{L}{r}\right)^{5/2}. \tag{7}$$

The above relation has a size effect due to the material intrinsic length $\Delta\gamma/E$ involved.

2.2. Collapse of parallel nanofibre segments

In this case, a pair of uniform fibre segments is considered. Similar to the above derivation, the asymptotic distance between deflected fibre segments (see figure 3) near the contact point can be expressed as

$$z = 6h\left[\left(\frac{2x}{L}\right)^2 - \frac{2}{3}\left(\frac{2x}{L}\right)^3\right] + \frac{y^2}{r} + h_0$$
$$\approx 6h\left(\frac{2x}{L}\right)^2 + \frac{y^2}{r} + h_0, \qquad (\text{for } x/L \ll 1) \tag{8}$$

where the (x, y)-coordinate system is selected following that in section 2.1. By using the adhesive force (6), it is

$$P = 4\int_A \sigma(z)\,\mathrm{d}A = \frac{\pi}{2\sqrt{6}}\Delta\gamma L\sqrt{r/h}. \tag{9}$$

Substituting (9) into (2) leads to the critical collapse distance h_c:

$$\left(\frac{h_c}{L}\right)^{3/2} = \frac{1}{96\sqrt{6}}\frac{\Delta\gamma}{Er}\left(\frac{L}{r}\right)^{5/2}. \tag{10}$$

For uniform fibre segments (i.e. $\gamma_1 = \gamma_2 = \gamma$ and $\gamma_{12} = 0$), the Dupré adhesion energy is reduced to $\Delta\gamma = 2\gamma$ and relation (10) becomes

$$\left(\frac{h_c}{L}\right)^{3/2} = \frac{1}{48\sqrt{6}}\frac{\gamma}{Er}\left(\frac{L}{r}\right)^{5/2}. \tag{11}$$

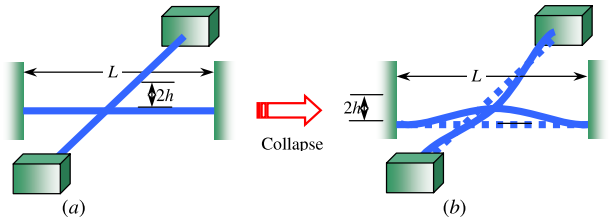

Figure 4. Adhesion between orthogonal fibre segments.

2.3. Collapse of orthogonal nanofibre segments

In this case, two fibre segments are still considered with the same geometries and material properties. Thus, the deflection shape (1) still holds for each fibre segment as illustrated in figure 4. Based on the derivation in section 2.1, the asymptotic distance between deflected fibre segments near the contact point is

$$\begin{aligned} z &= 3h\left[\left(\frac{2x}{L}\right)^2 - \frac{2}{3}\left(\frac{2x}{L}\right)^3\right] + 3h\left[\left(\frac{2y}{L}\right)^2 - \frac{2}{3}\left(\frac{2y}{L}\right)^3\right] \\ &\quad + \frac{x^2}{2r} + \frac{y^2}{2r} + h_0 \\ &\approx \left(\frac{12h}{L^2} + \frac{1}{2r}\right)(x^2 + y^2) + h_0 \\ &\quad (\text{for } x/L \ll 1 \text{ and } y/L \ll 1). \end{aligned} \tag{12}$$

Substituting (12) into (6) yields the adhesive force:

$$P = 4\int_A \sigma(z)\,\mathrm{d}A = \frac{2\pi\Delta\gamma r}{1 + 24hr/L^2}. \tag{13}$$

In the limiting case of two long, straight, rigid cylinders (i.e. $L \gg r$ or $L \gg h$), relation (13) covers those estimated using the Derjaguin approximation [44]. Consequently, plugging (13) into (2) leads to the quadratic characteristic equation of the system such that

$$\left(\frac{h}{L}\right)^2 + \frac{L}{24r}\left(\frac{h}{L}\right) - \frac{\Delta\gamma L^3}{24^2 E r^4} = 0. \tag{14}$$

The positive root of (14) gives the critical collapse distance h_c:

$$\frac{h_c}{L} = \frac{1}{48}\left[\sqrt{\left(\frac{L}{r}\right)^2 + \frac{4\Delta\gamma L^3}{Er^4}} - \frac{L}{r}\right]. \tag{15}$$

With the Dupré adhesion energy $\Delta\gamma = 2\gamma$ in this case, relation (15) can be recast into

$$\frac{h_c}{L} = \frac{1}{48}\left[\sqrt{\left(\frac{L}{r}\right)^2 + \frac{8\gamma L^3}{Er^4}} - \frac{L}{r}\right]. \tag{16}$$

Furthermore, for relatively large fibre radius, there exists a limiting critical collapse distance dependent only of the fibre aspect ratio L/r and the material intrinsic length (usually $\gamma/E < 1$ nm) such that

$$h_c = \frac{1}{12}\left(\frac{L}{r}\right)^3 \frac{\gamma}{E}. \tag{17}$$

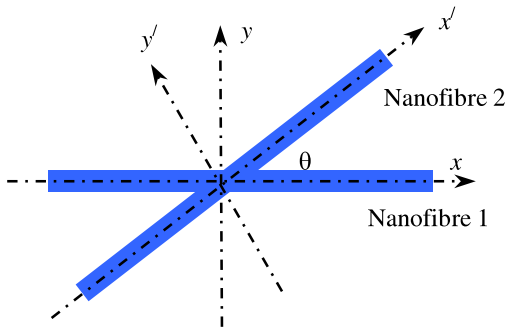

Figure 5. Geometries of fibres at arbitrary angle.

2.4. Collapse of fibre segments in arbitrary angle

Now let us consider two uniform fibre segments located in two parallel horizontal planes with distance h. The spatial angle between the fibre axes is denoted as θ. Simple relationships exist between two coordinate systems attached to the fibre axes as adopted in figure 5:

$$\begin{aligned} x' &= x\cos\theta + y\sin\theta, \\ y' &= -x\sin\theta + y\cos\theta. \end{aligned} \tag{18}$$

Obviously, in the first-order approach, the deflection shape (1) still holds for each nanofibre segment after collapse. By using the derivation in section 2.1, the asymptotic distance between deflected fibre segments near the contact point is

$$\begin{aligned} z &= 3h\left[\left(\frac{2x}{L}\right)^2 - \frac{2}{3}\left(\frac{2x}{L}\right)^3\right] + \frac{y^2}{2r} + 3h \\ &\quad \times \left[\left(\frac{2x'}{L}\right)^2 - \frac{2}{3}\left(\frac{2x'}{L}\right)^3\right] + \frac{y'^2}{2r} + h_0 \\ &\approx \frac{12h}{L^2}x^2 + \frac{y^2}{2r} + \frac{12h}{L^2}x'^2 + \frac{y'^2}{2r} + h_0 \\ &\quad (\text{for } x/L \ll 1 \text{ and } x'/L \ll 1). \end{aligned} \tag{19}$$

Substituting (18) into (19) yields the asymptotic distance in the (x, y) system such that

$$\begin{aligned} z &\approx \frac{12h}{L^2}\left[(1+\cos^2\theta)x^2 + \sin 2\theta xy + \sin^2\theta y^2\right] \\ &\quad + \frac{1}{2r}[\sin^2\theta x^2 - \sin 2\theta xy + (1+\cos^2\theta)y^2] + h_0 \\ &\quad (\text{for } x/L \ll 1 \text{ and } x'/L \ll 1). \end{aligned} \tag{20}$$

In the above, if letting $\theta = 0°$ and $\theta = 90°$, the asymptotic distance (20) recovers the ones given by (8) and (12), respectively. Furthermore, by using (20) to replace the distance z in (6), one can obtain the adhesive force:

$$\begin{aligned} P &= \int_\Gamma \sigma(z)\,\mathrm{d}A = \frac{8\Delta\gamma}{3\varepsilon}\int_{-\infty}^{+\infty}\int_{-\infty}^{+\infty}\left[\left(\frac{\varepsilon}{z}\right)^3 - \left(\frac{\varepsilon}{z}\right)^9\right]\mathrm{d}x\,\mathrm{d}y, \\ &= \pi\Delta\gamma L/\sqrt{D}, \end{aligned} \tag{21}$$

where D is the determinant of a positive-defined matrix relating the fibre aspect ratio L/r, fibre distance h_c and angle between fibres θ, i.e.

$$D = \begin{vmatrix} (1+\cos^2\theta)\frac{12h}{L} + \sin^2\theta\frac{L}{2r} & \sin\theta\cos\theta\left(\frac{12h}{L} + \frac{L}{2r}\right) \\ \sin\theta\cos\theta\left(\frac{12h}{L} + \frac{L}{2r}\right) & \sin^2\theta\frac{12h}{L} + (1+\cos^2\theta)\frac{L}{2r} \end{vmatrix}. \tag{22}$$

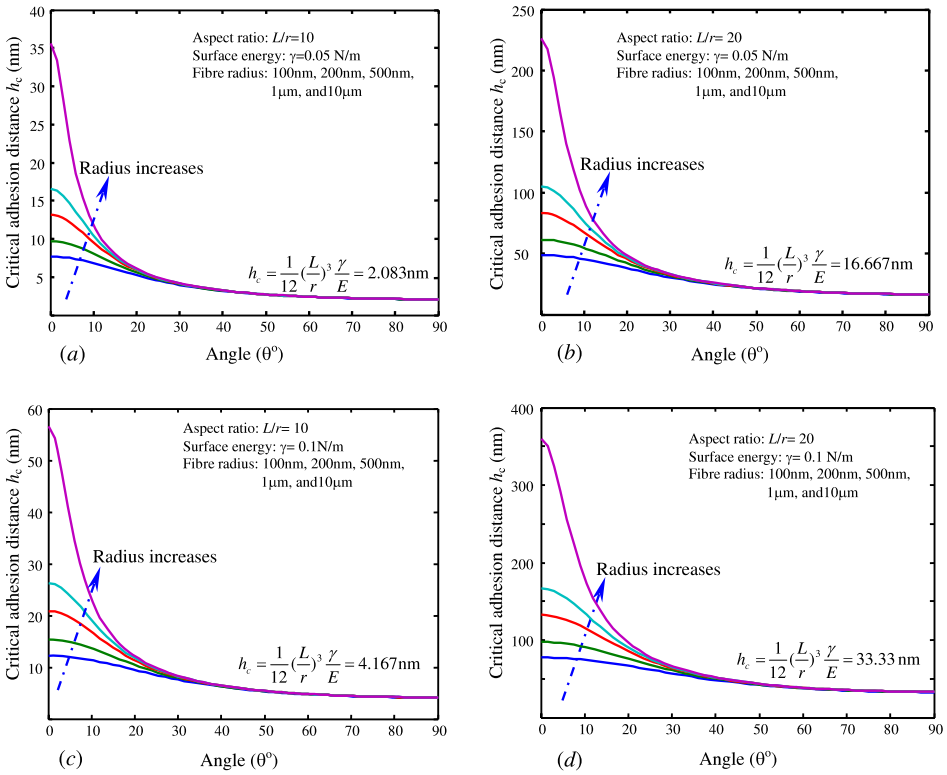

Figure 6. Variation of the critical collapse distance h_c between fibre segments versus angle θ at varying fibre radius r and aspect ratio L/r: (a) $L/r = 10$, $\gamma = 0.05$ N m^{-1}; (b) $L/r = 20$, $\gamma = 0.05$ N m^{-1}; (c) $L/r = 10$, $\gamma = 0.1$ N m^{-1}; and (d) $L/r = 20$, $\gamma = 0.1$ N m^{-1}.

Plugging (21) into (2) leads to the characteristic equation of the system such that

$$\frac{h_c}{L} = \frac{1}{48\sqrt{D}} \frac{\Delta\gamma}{Er} \left(\frac{L}{r}\right)^3. \tag{23}$$

Again, with the Dupré adhesion energy $\Delta\gamma = 2\gamma$ in this case, relation (23) can be rewritten as

$$\frac{h_c}{L} = \frac{1}{24\sqrt{D}} \frac{\gamma}{Er} \left(\frac{L}{r}\right)^3. \tag{24}$$

In the above, except for the special cases of $\theta = 0°$ and 90° as discussed in sections 2.2 and 2.3, for an arbitrary angle θ, it is unable to extract the critical collapse distance h_c in explicit form from (24). In this case, the numerical method for searching roots of polynomials has to be evoked.

3. Numerical results and discussions

With critical collapse criterion (24) involving the material intrinsic length γ/E or $\Delta\gamma/E$, we can draw the conclusion that the size effect of fibre radius on nanofibre collapse does exist. Hereafter, we evaluate the variation of the critical collapse distance h_c versus the fibre angle θ at varying surface energy γ, fibre aspect ratio L/r and fibre radius r. For convenience, relation (24) is recast into

$$\frac{h_c}{r} = \frac{1}{24\sqrt{D}} \frac{\gamma}{Er} \left(\frac{L}{r}\right)^4. \tag{25}$$

During the numerical process, fibre surface energies are selected as $\gamma = 0.05$ N m^{-1} and $\gamma = 0.1$ N m^{-1}, respectively, and Young's modulus is chosen as $E = 2$ GPa. These values are close to those of typical polymer fibres. Therefore, once parameters L, r and θ are given, equation (25) can be solved numerically for h_c. The h_c values for fibre segments of radii 100 nm, 200 nm, 500 nm, 1 μm and 10 μm, respectively, are plotted in figure 6, from which it can be found that the size effect of fibre radius exists. For a given fibre pair, the critical collapse distance h_c decreases rapidly with increasing angle θ, and simultaneously it also decreases with the increase of fibre surface energy. At fixed fibre aspect ratio L/r, at small angle θ, h_c increases with increasing fibre radius; however, at relatively large angle θ, h_c tends to a constant as given in (17), e.g. $(1/12)(L/r)^3\gamma/E$. This constant depends only upon the aspect ratio L/r and the material intrinsic length $\gamma/E = 0.025$ nm for $\gamma = 0.05$ N m^{-1}, and $\gamma/E = 0.05$ nm for $\gamma = 0.1$ N m^{-1}. This parameter is expected to be very useful for collapse analysis and design of nanofibre networks and nanofibre devices. Furthermore, at fixed fibre radius, h_c grows significantly with increasing aspect ratio L/r. This is because the bending stiffness of a fibre segment decreases rapidly with the increase of fibre segment length following a reciprocal cubic law.

In reality, nanofibre segments within a fibre network usually have very high aspect ratio. Due to the small diameter of nanofibres, the above analysis implies that nanofibre networks are generally more unstable than those made of thick fibres. Numerical simulation also indicates that parallel fibres have the maximum h_c value due to their greatest adhesive

force, while orthogonal fibres have the minimum h_c value. This is a reasonable explanation of the nanofibre collapse phenomena observed in experiments.

Nevertheless, it should be mentioned that surface adhesion in a real fibre network is much more complex. In particular, near the fibre contacts where two or more fibres intersect, the adhesion calculation would be more complicated. Fixed boundary conditions adopted above are also a strict assumption. Consequently, all the above calculations of adhesive force are based on a modified Bradley's approach; therefore the adhesion energy of post-collapse (with greater contact areas) is much greater than the initial adhesion energy in inducing the initial nanofibre collapse (adhesion) of nanofibres as considered in this work.

4. Conclusions

In this paper, adhesion-induced micro/nanofibre collapse has been studied. The critical collapse distance between neighbouring fibre segments has been derived for typically four fibre collapse modes. Relation (24) is the general criterion for adhesion-induced collapse of fibres. Based on this relation, effects of fibre elasticity, surface adhesion and fibre geometries on the critical collapse distance have been explored. Due to the involvement of the material's intrinsic length $\Delta\gamma/E$ or γ/E in (23) and (24), the fibre collapse condition has a size effect. The calculation of the adhesive force in the present study is based on Bradley's approach, which does not consider the deformation induced by adhesion. However, this approach did not affect the present results for only considering the critical condition of initial fibre collapse.

Furthermore, although the present study is based on two uniform micro/nanofibre segments, the method developed above can be naturally extended in examining the collapse mechanisms and criteria of micro/nanofibre networks made of dissimilar fibres (e.g. with dissimilar material properties, geometries, etc) and other microstructures such as MEMS/NEMS and slender rubber stamps used in soft lithography.

Acknowledgments

Partial support of this study by the US NSF, AFOSR and ARO/ARL is gratefully acknowledged. The authors would like to thank the anonymous reviewers for their enlightening comments and helpful suggestions to improve the paper.

References

[1] Reneker D H and Chun I 1996 *Nanotechnology* **7** 216
[2] Dzenis Y 2004 *Science* **304** 1917
[3] Li D and Xia Y N 2004 *Adv. Mater.* **16** 1151
[4] Huang C B, Chen S L, Lai C L, Reneker D H, Qiu H, Ye Y and Hou H Q 2006 *Nanotechnology* **17** 1558
[5] Kim J S and Reneker D H 1999 *Polym. Compos.* **20** 124
[6] Dzenis Y A and Reneker D H 2001 *US Patent Specification* 626533
[7] Dzenis Y A and Wen Y K 2002 *Mater. Res. Soc. Symp. Proc.* **702** 173
[8] Wu X F 2003 Fracture of advanced polymer composites with nanofiber reinforced interfaces *PhD Thesis* University of Nebraska, Lincoln, USA
[9] Huang Z M, Zhang Y Z, Kotaki M and Ramakrishna S 2003 *Compos. Sci. Technol.* **63** 2223
[10] Zhang Y Z, Lim C T, Ramakrishna S and Huang Z M 2005 *J. Mater. Sci. Mater. Med.* **16** 933
[11] Chew S Y, Wen Y, Dzenis Y and Leong K W 2006 *Curr. Pharm. Des.* **12** 4751
[12] van Wyk C M 1946 *J. Textile Inst.* **37** T285
[13] Cox H L 1952 *Brit. J. Appl. Phys.* **3** 72
[14] Pan N and Carnaby G A 1989 *Textile Res. J.* **59** 285
[15] Carnaby G A and Pan N 1989 *Textile Res. J.* **59** 275
[16] Komori T and Itoh M 1991 *Textile Res. J.* **61** 420
[17] Komori T and Itoh M 1991 *Textile Res. J.* **61** 588
[18] Komori T, Itoh M and Takaku A 1992 *Textile Res. J.* **62** 567
[19] Lee D H and Carnaby G A 1992 *Textile Res. J.* **62** 185
[20] Niskanen K J and Alava M J 1994 *Phys. Rev. Lett.* **73** 3475
[21] Astrom J, Saarinen S, Niskanen K and Kurkijarvi J 1994 *J. Appl. Phys.* **75** 2383
[22] Pan N, Chen J, Seo M and Backer S 1997 *Textile Res. J.* **67** 907
[23] Wang C, Cheng X, Sastry A M and Choi S B 1999 *ASME J. Eng. Mater. Technol.* **121** 503
[24] Narter M A, Batra S K and Buchanan D R 1999 *Proc. R. Soc.* A **455** 3543
[25] Astrom J A, Makinen J P, Alava M J and Timonen J 2000 *Phys. Rev.* E **61** 5550
[26] Astrom J A, Makinen J P, Hirvonem H and Timonen J 2000 *J. Appl. Phys.* **88** 5056
[27] Wang C W, Berhan L and Sastry A M 2000 *ASME J. Eng. Mater. Technol.* **122** 450
[28] Wang C W and Sastry A M 2000 *ASME J. Eng. Mater. Technol.* **122** 460
[29] Sastry A M, Wang C W and Berhan L 2001 *Key Eng. Mater.* **200** 229
[30] Berhan L, Yi Y B and Sastry A M 2004 *J. Appl. Phys.* **95** 5027
[31] Berhan L, Yi Y B, Sastry A M, Munoz E, Selvidge M and Baughman R 2004 *J. Appl. Phys.* **95** 4335
[32] Wu X F and Dzenis Y A 2005 *J. Appl. Phys.* **98** 093501
[33] Chatterjee A P 2006 *J. Appl. Phys.* **100** 054302
[34] Wu X F and Dzenis Y A 2006 *J. Appl. Phys.* **100** 124318
[35] Bradley R S 1932 *Phil. Mag.* **13** 853
[36] Johnson K L, Kendall K and Roberts A D 1971 *Proc. R. Soc.* A **324** 301
[37] Derjaguin B V, Muller V M and Toporov Y P 1975 *J. Colloid Interface Sci.* **53** 314
[38] Tabor D 1977 *J. Colloid Interface Sci.* **58** 2
[39] Greenwood J A 1997 *Proc. R. Soc.* A **453** 1277
[40] Zhao Y P, Wang L S and Yu T X 2003 *J. Adhes. Sci. Technol.* **17** 519
[41] Shi X H and Zhao Y P 2004 *J. Adhes. Sci. Technol.* **18** 55
[42] Muller V M, Yushchenko V S and Derjaguin B V 1980 *J. Colloid Interface Sci.* **77** 91
[43] Maugis D 1992 *J. Colloid Interface Sci.* **150** 243
[44] Israelachvili J 1992 *Intermolecular and Surface Forces* 2nd edn (New York: Academic)